

# Detection and tracking of defects in the gyroid mesophase

Jens Harting <sup>a</sup>, Matthew J. Harvey <sup>b</sup>, Jonathan Chin <sup>b</sup>,  
Peter V. Coveney <sup>b</sup>

<sup>a</sup>*Institute for Computational Physics, University of Stuttgart, Pfaffenwaldring 27,  
D-70569 Stuttgart, Germany*

<sup>b</sup>*Centre for Computational Science, Christopher Ingold Laboratories, University College  
London, 20 Gordon Street, London WC1H 0AJ, UK*

---

## Abstract

Certain systems, such as amphiphile solutions or diblock copolymer melts, may assemble into structures called “mesophases”, with properties intermediate between those of a solid and a liquid. These mesophases can be of very regular structure, but may contain defects and grain boundaries. Different visualization techniques such as volume rendering or iso-surfacing of fluid density distributions allow the human eye to detect and track defects in liquid crystals because humans are easily capable of finding imperfections in repetitive spatial structures. However, manual data analysis becomes too time consuming and algorithmic approaches are needed when there are large amounts of data. We present and compare two different approaches we have developed to study defects in gyroid mesophases of amphiphilic ternary fluids. While the first method is based on a pattern recognition algorithm, the second uses the particular structural properties of gyroid mesophases to detect defects.

*Key words:* Gyroid cubic mesophase, liquid crystal, defect analysis.

*PACS:* 61.30.Jf, 61.72.Bb, 83.10.Lk

---

## 1 Introduction

Molecules in an ordinary liquid will usually have random orientations. There is a certain interesting class of liquids, called liquid crystals, in which this is not the case: the molecules exhibit a tendency to align or order. Liquid crystals have some of the properties of crystals, since they exhibit long-range ordering and strong anisotropy, but retain the ability to flow, unlike ordinary crystals in which the molecules are locked onto well-defined positions on a lattice.

Amphiphiles are one class of molecule which may produce liquid crystalline behaviour. These are molecules constructed from two parts, usually a water-loving head and a long tail which is attracted to oil. In a mixture of oil, water, and amphiphile, amphiphile molecules are attracted to the interface between the oil and water to minimize free energy, hence they are often termed “surface active agents”, or surfactants. Their precise behaviour is strongly dependent on concentration, so they are termed “lyotropic” liquid crystals.

A random mixture of oil, water, and surfactant molecules will often spontaneously arrange itself into separate regions of oil and water, separated by a layer of surfactant at the interface, forming structures called surfactant mesophases. These structures can be very complex, and their geometry depends strongly upon the relative proportions of different molecules in the mixture, and the details of how they interact. Such structures can also be produced in binary systems, such as water-lipid mixtures, and often occur in biological systems[1,2,3].

Surfactant mesophases will often form minimal surfaces: for any boundary drawn on the surface, the surface lying inside the boundary will have the minimal possible surface area, and the surface will also have zero mean curvature. Triply periodic minimal surfaces[4] which extend through space with cubic symmetry[5] have been found in many systems, such as lipid-water mixtures[1], diblock copolymers[6], and in many biological systems[7].

The gyroid, also known as the “G surface”, is a particular minimal surface, discovered by Schoen[8]. It is embedded (has no self-intersections), triply periodic (repeats in  $x$ ,  $y$ , and  $z$  directions), and is the only known such surface with triple junctions (Figure 1(b)). A numerical study of the gyroid was made by Große-Brauckmann[9]; while an analytical description was found by Gandy and Klinowski[10] a very close approximation of a gyroid is the surface  $\cos x \sin y + \cos y \sin z + \cos z \sin x = 0$ . It is possible to transform the gyroid into two other well-known surfaces, the P and D surfaces, through the single parameter known as the Bonnet Angle[11]. The gyroid has symmetry group  $Ia\bar{3}d$ ; the unit cell consists of 96 copies of a fundamental surface patch, related through the symmetry operations[10] of this space group.

The gyroid surface divides space into two interpenetrating regions, or labyrinths. In the case of gyroids formed from a mixture of oil, water, and surfactant, one labyrinth contains mostly oil, the other mostly water, and the gyroidic boundary surface between the two labyrinths is populated with surfactant, as shown in Figure 1(a) and 1(b).

Channels run through the gyroid labyrinths in the (100) and (111) directions; passages emerge perpendicular to any given channel as it is traversed, the direction at which they do so gyrating down the channel, giving rise to the “gyroid” name[9].

The labyrinths are chiral, so that the channels of one labyrinth gyrate in the op-

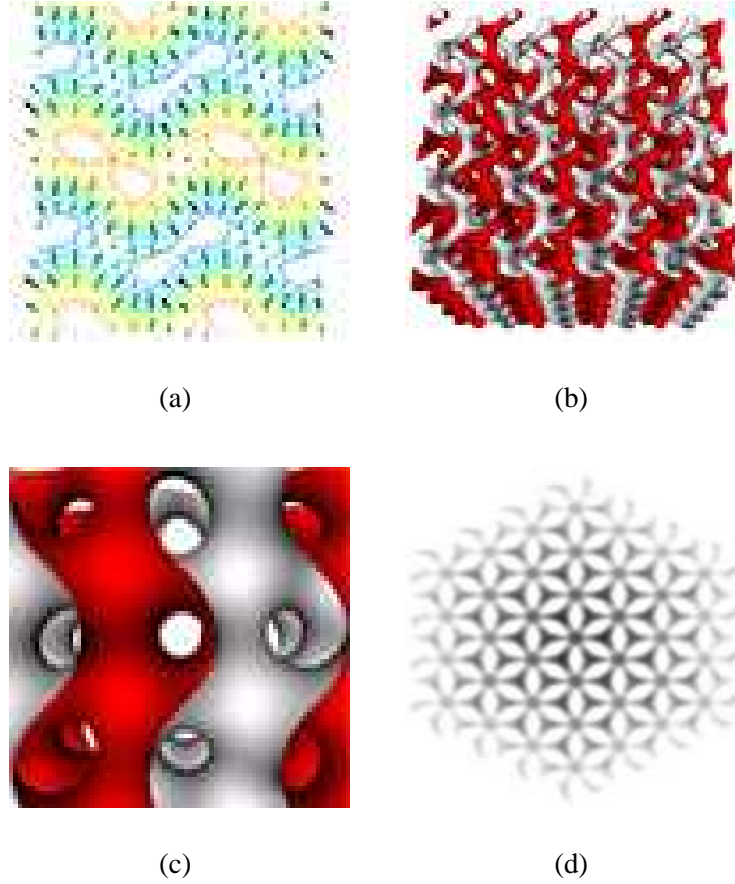


Fig. 1. Views of the gyroid mesophase. 1(a) 2D slice from a small ( $16^3$ ) simulation of a gyroid mesophase. Contours show composition, varying from pure oil to pure water; arrows show the surfactant orientation. It can be seen clearly that the surfactant sits at the interface, with the head groups pointing towards the water component. 1(b) Structure of the two labyrinths enclosed by a gyroid minimal surface, showing the characteristic triple junctions. 1(c) Channels running in the (100) direction of a gyroid surface: note how adjacent channels rotate in opposite senses. 1(d) Parallel-projection volume rendering of a gyroid, looking in the (111) direction to show the distinctive “wagon-wheel” appearance.

posite sense to the channels of the other, as seen in Figure 1(c). Looking down the (111) direction of a gyroid shows a distinctive “wagon wheel” pattern (Figure 1(d)), which has been observed experimentally in transmission electron micrographs of gyroid phases[6].

As a Platonic or mathematical abstraction, the gyroid consists of perfect copies of the unit cell, repeating on a Bravais lattice extending through space. This is not the case for gyroid structures in the real world: various effects may give rise to regions where the structure deviates from a gyroid. Such deviations are called *defects*.

During the gyroid self-assembly process, several small, separated gyroid-phase regions or domains may start to form, and then grow. Since the domains evolve inde-

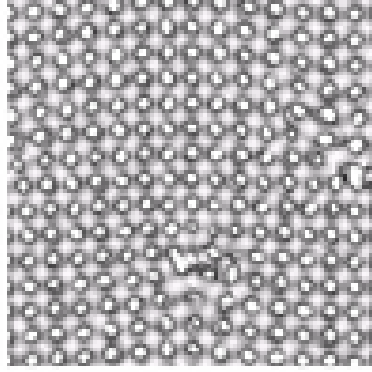


Fig. 2. Dislocation in a simulated gyroid mesophase

pendently, the lattices describing them may not be identical, and can differ in orientation, position, or unit cell size. The interface between the domains will not be gyroidal: therefore, grain-boundary defects arise between gyroid domains. Inside a domain, there may be dislocations, or line defects, corresponding to the termination of a plane of unit cells; there may also be localised non-gyroid regions, corresponding to defects due to contamination or inhomogeneities in the initial conditions.

While equilibrium gyroid mesophases and their defects are observed experimentally, it is desirable to formulate a theoretical or computational model to better understand how and why they form and how they evolve.

Much effort has been invested in theoretical and computational modelling of liquid crystals. Nematic liquid crystals have been modelled using the Leslie-Erickson formulation [12]; Monte Carlo[13,14] and Molecular Dynamics[15] simulations have provided some insight, but reaching regimes where hydrodynamic effects are significant is currently computationally unfeasible with these techniques.

Lyotropic liquid crystals, of interest in this paper, have also been studied extensively[16] through techniques such as free-energy methods[17,18] and through consideration of the interface between the lipid and water phases[19]; again, most treatments have been limited to examination of the equilibrium state and its stability.

There have been recent attempts to take advantage of the lattice Boltzmann method for hydrodynamics[20,21], and modify it to take account of liquid-crystalline behaviour. Lattice Boltzmann is a discrete-time and discrete-space algorithm; since only nearest-neighbour interactions take place between vertices on the simulation lattice, it is extremely fast, and extremely scalable on parallel computer hardware[22]. There are several such schemes, some of which[23] are based around the Leslie-Ericksen model for nematic liquid crystals, and others which use a free-energy-based approach for nematic[24,25,26,27,28,29] and lyotropic[30,31] phases.

We used another kind of lattice Boltzmann model, which employs a “bottom-up” approach to model interactions between particles[32,33] including surfactants[34],

postulating a form of interparticle potential rather than using a free-energy-based technique. Briefly, the single-particle distribution function  $f_i^\sigma(\mathbf{x})$  for species  $\sigma$  with velocity  $\mathbf{c}_i$  is discretized onto lattice points  $\mathbf{x}$ , and then evolved according to the lattice BGK equation[21]. Three species, called red, blue, and green, are used, corresponding to oil, water, and surfactant. Immiscible fluids are modelled using an interparticle interaction force, controlled by a coupling constant  $g_{cc}$ : this force is calculated from the gradient of the order parameter, or “colour field”, defined as the difference  $\phi(\mathbf{x}) = \rho^r(\mathbf{x}) - \rho^b(\mathbf{x})$  between red and blue fluid densities. The mean surfactant director field  $\mathbf{d}(\mathbf{x})$  is also tracked on the lattice. A point-like surfactant molecule is modelled as being constructed from two different immiscible fluid molecules joined together, and therefore subject to dipole-like interactions with the other fluids, controlled by a coupling constant  $g_{cs}$ . Finally, interactions between surfactant molecules are controlled by a constant  $g_{ss}$ . It was recently shown[35,36] through simulations with the LB3D parallel lattice Boltzmann code that certain mixtures of specific composition (specified by the initial densities  $f_r, f_b, f_g$  of oil, water, and surfactant) would spontaneously assemble from a randomized, disordered initial condition, into a gyroid mesophase whose lattice parameter is around 8–9 simulation lattice sites. Similar cubic phases have been observed experimentally with lattice parameter of order 50nm, in polymer blends[6] and biological systems[7].

On a sufficiently small lattice, the gyroid may evolve to perfectly fill the simulated region, without defects. As the lattice size grows, it becomes more probable that multiple gyroid domains will emerge independently, so that grain boundary defects are more likely to appear and the time required for localized defects to diffuse across the lattice increases making it more likely that defects will persist. Therefore, examination of the defect behaviour of surfactant mesophases requires the simulation of very large systems. This was achieved as part of the TeraGyroid project, where systems on lattice sizes of up to  $1024^3$  were simulated by linking together multiple geographically-distributed supercomputing resources to form a computational Grid[37,38,39,40].

## 2 Structure factor analysis of liquid gyroid mesophases

Simulation data from liquid crystal dynamics can be visualized using isosurfacing or volume rendering techniques. The human eye has a remarkable ability to easily distinguish between regions where the crystal structure is well developed and areas where it is not. For quantitative studies of large systems evolving over long intervals of time, computational methods for defect detection and tracking are required. Developing algorithms to detect and track defects is a non-trivial task, however, since defects can occur within and between domains of varying shapes and sizes and over a wide variety of length and time scales.

A standard method to analyse simulation data is the calculation of the three-dimensional structure function

$$S(\mathbf{k}, t) \equiv \frac{1}{V} |\phi'_{\mathbf{k}}(t)|^2, \quad (1)$$

where  $V$  is the number of sites of the lattice,  $\phi'_{\mathbf{k}}(t)$  the Fourier transform of the fluctuations of the order parameter  $\phi' \equiv \phi - \langle \phi \rangle$ , and  $\mathbf{k}$  is the wave vector [41,36].  $S(\mathbf{k}, t)$  can easily be calculated, but only gives general information about the crystal development [42,43,35]. It does not allow one to detect where the defects are located or how many there are, nor does it furnish access to information about the number of differently oriented gyroid domains.

Figure 3 gives an example of the three-dimensional structure factor calculated for the order parameter  $\phi(\mathbf{x})$  at timesteps  $t=10000$ ,  $100000$ , and  $700000$ . We use periodic boundary conditions, a  $128^3$  lattice and simulate for one million timesteps. This is more than an order of magnitude longer than any other simulation performed before the TeraGyroid [40] project using our lattice-Boltzmann code LB3D and took 300 wall clock hours on 128 CPUs of an IBM SP4 (namely HPCx in Daresbury, UK). We use data from this simulation throughout the present paper to demonstrate the properties of different defect detection and tracking algorithms. The initial condition of the simulation is a random mixture with maximum densities of 0.7 for the case of the immiscible fluids and 0.6 for surfactant. The surfactant-surfactant coupling constant is given by  $g_{ss}=-0.0045$  and the coupling between surfactant and the other fluids is determined by  $g_{cs}=-0.006$ . In order to obtain a visualization that is comparable to experimentally obtained SAXS data (see for example [42]), we sum the structure factor in one of the cartesian directions. The example here has been summed in the  $x$ -direction and  $X_{max}$  denotes the value of the largest peak normalised by the number of lattice sites in the direction of summation (128 in this case). Results for the  $y$ - and  $z$ -directions are similar. At  $t=10000$ , gyroid assembly is just commencing, which is evident due to the eight peaks of the structure factor which are already clearly distinguishable.  $X_{max}$  is 11.85 in this case and is almost eight times bigger for  $t=100000$ . The peaks of the structure function correspond to a well developed crystal which consists of differently oriented gyroid domains with defects at the domain boundaries. At  $t=700000$ ,  $X_{max}$  reaches 197.00 and most of the previously existing domains have merged into a single one. Only a few defects are left of which two can be spotted visually at the right corner of the volume rendered visualisation and the centre of the top surface (denoted by the white arrows).

We are interested here in very well developed liquid crystals with defect domains covering only a minority of the total simulation volume. In order to distinguish between different defects and to study their evolution in time, we need to be able to clearly separate defect domains from regions where we find a perfect gyroid structure. An important property of these systems is that the variations of the structure function in time become very small and the system reaches a state close to equilibrium. Figure 4 shows the time dependence of the maxima of the structure func-

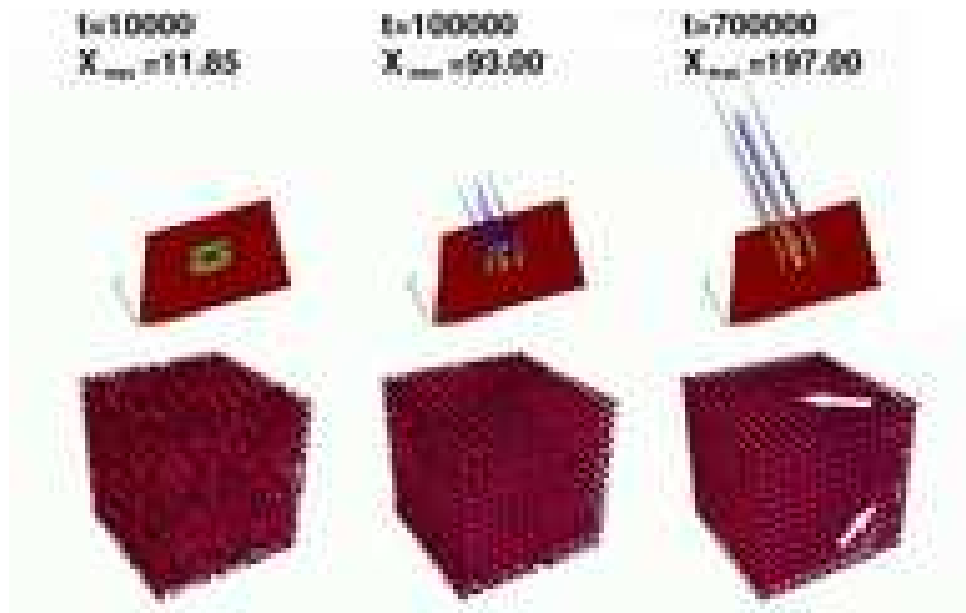


Fig. 3. Three-dimensional structure factor of the order parameter at timesteps  $t=10000$ ,  $100000$ , and  $700000$ , lattice size  $128^3$  and simulation parameters  $f_r=f_b=0.7$ ,  $f_g=0.60$ ,  $g_{ss}=-0.0045$ ,  $g_{cs}=-0.006$ . For comparability with SAXS experimental data, we display the total structure factor in the  $x$ -direction  $X=\sum_{k_x} S(\mathbf{k}, t)$ .  $X_{max}$  denotes the value of the largest peak divided by the number of lattice sites in the direction of summation (128 in this case). The lower half of the figure shows volume rendered visualizations of the corresponding order parameters and the white arrows are a guide for the eye to spot some defective areas at the top surface and the right corner at  $t=700000$ .

tion in  $x$ -,  $y$ - and  $z$ -direction for up to 700000 timesteps. To suppress short lived fluctuations within the fluid mixture, i.e. local variations that spontaneously form and disappear after up to a few thousand timesteps, we average every data point over 20000 timesteps. The maximum value of  $S(\mathbf{k}, t)$  shows a generally increasing behaviour in all three cases, but fluctuates greatly for the first 320000 timesteps. Then,  $X_{max}(t)$  and  $Z_{max}(t)$  show a steep increase indicating that two major gyroid domains are merging into a single one. During this process, defects located at the boundaries between these domains disappear. At  $t=400000$ , the fluctuations present in all three plots become very small indicating a very clean crystal with only a small number of defects. It is easy to detect this state numerically by defining a maximum allowed variation of the maximum values of the structure function. The remaining part of this paper will only discuss the analysis of data obtained for  $t \geq 340000$ .

Very long simulations like the one presented here can generate large amounts of data – especially if one measures physical quantities with a high resolution. Here, we measured the order parameter every 100 timesteps resulting in 10000 data files or about 78GB of data which we need to analyse. Filtering out data that is irrelevant for studying defect behaviour using the method described here allows us to reduce the number of files to 6500.

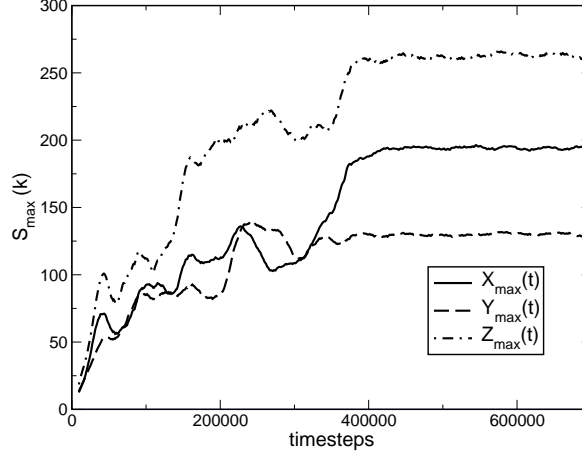


Fig. 4. Maximum value of the three orthogonal projections of the three-dimensional structure factor. For a clearer presentation, we averaged over 20000 timesteps to obtain a single data point displayed here.

### 3 Data reduction: From three dimensions to two dimensions

A first order approach to reduce the amount of data which needs to be analysed in detail is to project the three-dimensional system onto a two-dimensional plane. If one volume renders the order parameter of a gyroid unit cell using a step function which fills out all areas above an appropriate threshold value and leaves all values below that threshold transparent, it is possible to “look through” the unit cell under various angles. Since in a perfect gyroid mesophase the individual unit cells assemble in a very regular way, it is then possible to look through the whole liquid crystal. This can be implemented as a ray-tracing algorithm: First, select an appropriate projection direction, for example  $y$ . Define a projection plane  $P(x, z)$  to store the results and define a threshold value  $C$ . For the gyroid mesophase, we use 66% of the maximum value of the order parameter, but this value depends on the system to be analysed. For every point in the  $xz$ -plane, start at  $y=0$  and check for all values of  $y$  if the order parameter  $\phi(x, y, z)$  is smaller than  $C$ . As long as that is the case, we keep  $P(x, z)=0$ . If  $\phi(x, y, z)$  is greater or equal  $C$ , we set  $P(x, z)=1$ , move to the next point in the  $xz$ -plane and start from  $y=0$  again.

Figure 5 shows visualizations of  $P(x, z)$  for timesteps 50000, 100000, 200000, 300000, 400000, 500000, 600000, 700000. Black areas correspond to  $P(x, z)=1$  and white areas to  $P(x, z)=0$ . For early simulation times most of  $P(x, z)$  is 1 and while the simulation evolves white spots start to occur in the images presented in figure 5 until a very regular lattice-like structure with some black islands appears for  $t > 400000$ . Areas of regular lattice structure correspond to perfect crystal structures along the projection direction. Black islands can be interpreted as areas where the gyroid structure is disturbed or not existent at some point along the projection axis.

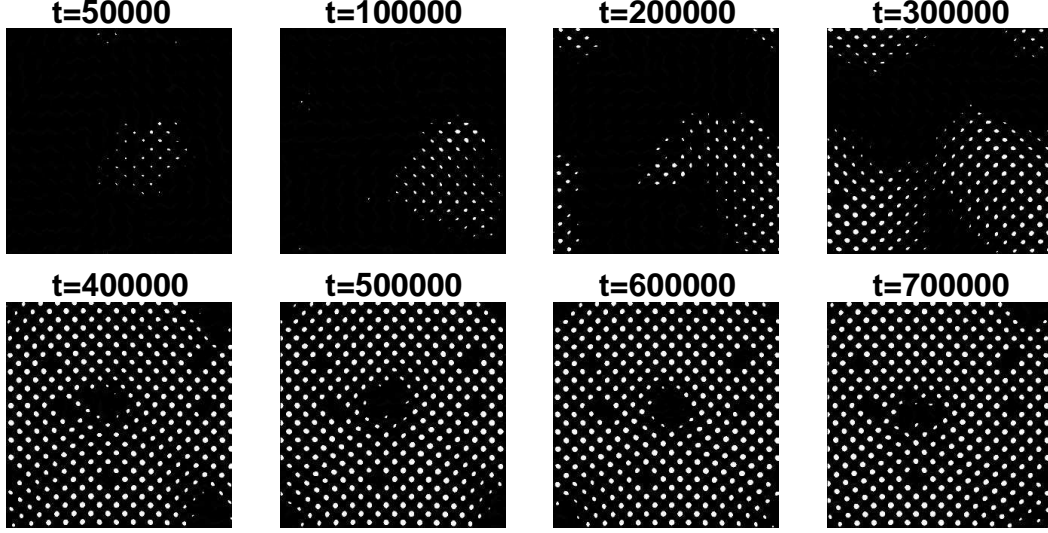


Fig. 5. Two-dimensional projection in the  $y$ -direction of volume rendered three-dimensional colour fields at  $t= 50000, 100000, 200000, 300000, 400000, 500000, 600000, 700000$ .

Obviously, projecting the full system makes it impossible to retain the three-dimensional structure of individual defects. Therefore, we apply the projection algorithm on slabs of the dataset only. For an optimal resolution of the defect detection, the slab thickness  $l$  should be comparable to the size of a gyroid unit cell which corresponds to eight lattice sites in our case, resulting in 16 individual  $128 \times 128 \times 8$  slabs for a  $128^3$  lattice. We found that using overlapping slabs does not improve the defect detection rate. The positions and sizes of the defects detected in the two-dimensional projections can be used to reconstruct three-dimensional datasets which only include the defective areas. A defective area in the two-dimensional datasets is mapped to a volume of thickness  $l$ .

In order to further improve the reliability of the detection, we repeat the analysis for all three cartesian directions. In this way, we can detect gyroid cells which are deformed in one direction only. For the reconstruction of the three-dimensional dataset, all three analysis runs are taken into account. Additional resolution can be obtained by distinguishing between how often and in which direction(s) a defective volume has been detected, indicating the particular kind of defect.

The human eye is easily able to accurately detect defective areas in the individual images of figure 5. In the following sections we will present two possible approaches which try to transfer this remarkable ability to a well defined algorithm that can be implemented on a computer. The first approach is based on a generic pattern recognition algorithm and should work with all liquid crystals that form a regular pattern, while the second has been developed with our particular problem in mind and is not known to work with systems other than the gyroid mesophase. However, it is about an order of magnitude faster and the general principles underlying it should be applicable to different systems as well.

## 4 A general pattern recognition based approach for the detection of defects

The first approach is based on the regularity or periodicity of patterns and was developed by Chetverikov and Hanbury in 2001 [44]. It is assumed that the defect-free pattern is homogeneous and shows some periodicity. The algorithm searches for areas which are significantly less regular (i.e. aperiodic) than the bulk of the dataset by computing regularity features for a set of windows and identifying defects as outliers in regularity feature space. The regularity is quantified by computing the periodicity of the normalised autocorrelation function in polar coordinates. In short, for every window a regularity value is computed. If this value differs by more than a defined threshold value from the median of all window regularity values, the area is accordingly classified as a defect. For a more detailed description of the algorithm see [44,45].

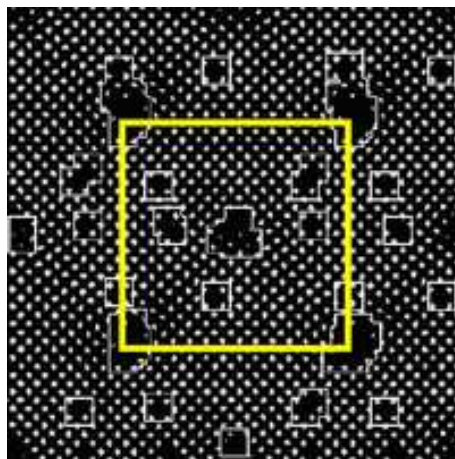


Fig. 6. Two-dimensional projection of the three-dimensional colour field for a gyroid system of size  $128^3$  at  $t=600000$ . The white frames depict the areas detected by the pattern recognition algorithm of Chetverikov and Hanbury [44]. In order to detect small defects at the system's boundaries, we extend the dataset by mirroring 50% of its corresponding content from the opposite side. The size of the original dataset is depicted by the large box.

We have found this pattern recognition algorithm to be very robust and reliable in detecting defects. In figure 6 the detected defects for an example dataset at  $t=600000$  are depicted by the white boxes. For good results, the regular pattern needs to occur multiple times within an analysis window. A window size of  $17 \times 17$  lattice sites has been found to generate the best results. Defects located in the central area of the crystal are very well detected, but the algorithm fails at the boundaries. We overcome this problem by taking advantage of the fact that our model has periodic boundary conditions, and extend the dataset by mirroring 50% of its corresponding content from the opposite side. In this way we increase the number of analysis windows containing regular patterns and the defects at the boundaries differ more substantially from the surrounding regular pattern since they appear at their full size. The pattern recognition algorithm is then able to detect boundary defects and, depending on the maximum size of defects, the size of the additional

“padded” regions can be adapted in order to limit the additional computational costs.

By applying the pattern recognition algorithm to all individual projected slabs of the dataset, we are able to reconstruct a three-dimensional volume that only consists of areas which have been detected as defective. Figure 7 shows reconstructed datasets at  $t=340000$ , 500000 and 999000. Even at  $t=340000$  a very large region of the system has not yet formed a well defined gyroid phase. 160000 timesteps later, the main defects are pillar shaped ones at the centre and at the corners of the visualised systems. Due to the periodic boundary conditions, the corner defects are connected and should be regarded as a single one. As can be seen from the analysis at  $t=999000$ , defects in the gyroid mesophase are very stable in size as well as in their position.



Fig. 7. Volume rendered visualization of the colour field at  $t=340000$ , 500000, 999000 from the evolving gyroid system. Only the defects are shown as they have been isolated from the full datasets using the pattern recognition algorithm.

## 5 A mesh generator as an alternative method for defect detection

The second approach presented in this paper also utilises the two-dimensional slab projections and encapsulates knowledge about the patterns produced by regular and defect regions (see figure 8). As a consequence, it is an order of magnitude faster than the pattern recognition code.

For each slab image, the centroid and area of each dot is computed and dots below a certain threshold area are discarded. The four nearest neighbours of each dot are determined and a connection mesh is generated (Figure 8(b)). Neighbours that lie more than one gyroid unit cell width away from a dot are discounted. Periodic boundary conditions are assumed when generating the mesh so that defects at the edge of the system may be reliably detected. Nodes which lie in defect-free regions of the lattice are distinguished by having four four-hop closed routes through neighbouring nodes (denoted by the arrows in figure 9). Mesh nodes that describe

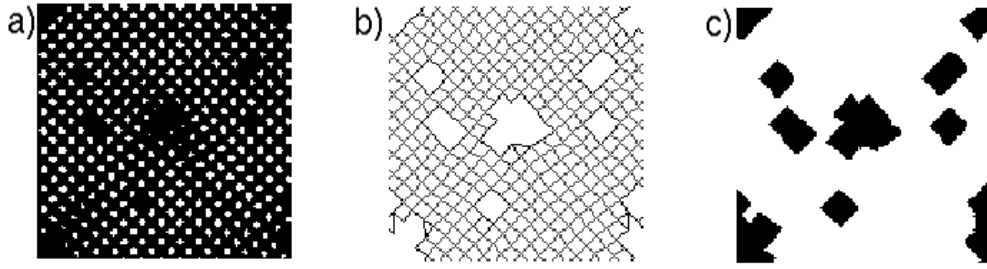


Fig. 8. Defect regions (c) are extracted from a mesh representation (b) of the two-dimensional projection (a) for  $t=600000$  shown in Figure 5.

the perimeter of defect regions lack this property. A tree-searching algorithm is used to search the data-structure representing the mesh and detect the presence of closed loops. The regions of regular mesh are discarded, leaving only mesh that describes the perimeters of defect regions (emboldened regions in 8(b)).

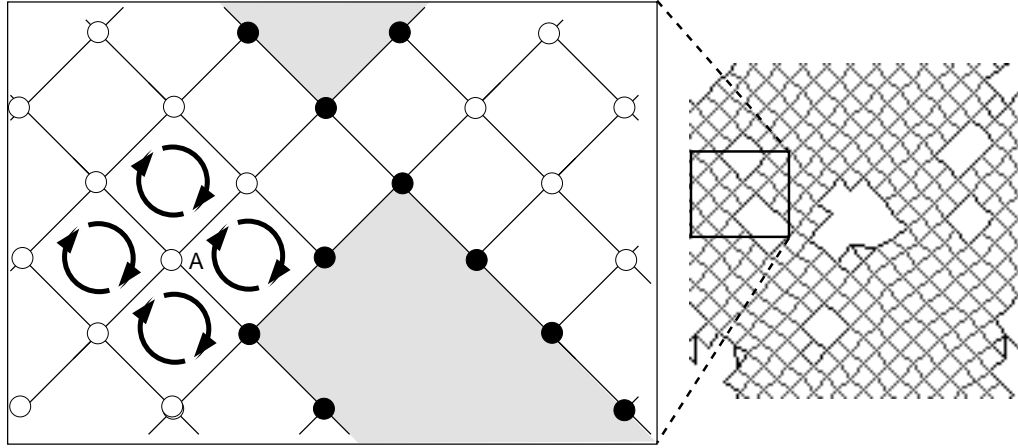


Fig. 9. Mesh nodes which lie within regular regions (A) are distinguished by having four four-hop closed routes through their neighbouring nodes. Nodes lacking this property (black) are categorised as defect boundary nodes.

A flood-fill algorithm is applied to a rasterised image of the defect perimeters to locate distinct defect regions and isolate them from the background (corresponding to defect-free regions). Thereafter, a mask image as presented in Figure 8(c) is generated.

As with the pattern recognition approach, this procedure is repeated for each of the three Cartesian axes and the resultant mask images are assembled to produce a three-dimensional defect mask which is then applied to the original dataset. For comparison, figure 10 shows reconstructed visualizations of defective areas for the same parameters and timesteps as figure 7.

Since the algorithm defines the perimeter of a defect region by the nearest mesh nodes, there is a tendency to over-estimate the boundary of the defect region. How-

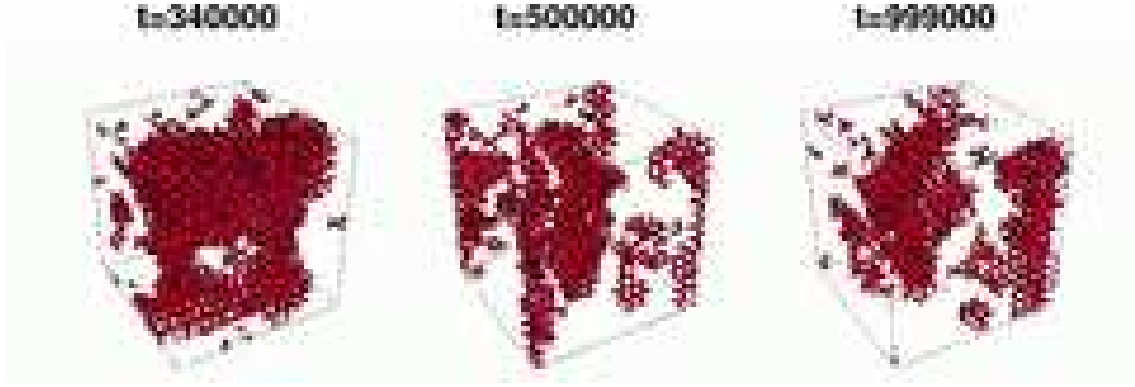


Fig. 10. Volume rendered visualization of the colour field at  $t=340000$ ,  $500000$ ,  $999000$  from the evolving lattice-Boltzmann simulation. Only the defects are shown as they have been separated from the full datasets using the mesh generation algorithm.

ever, this over-estimate is proportional to the defect surface area and the maximum error of the detected defect volume can be estimated as the volume of a one gyroid unit cell thick layer surrounding all individual defects.

Since the dots in the two-dimensional projections are sections of tube-like structure that run through the gyroid rather than spatially localised entities, the division of the dataset into slabs is an essential step. For this reason, no attempt was made to develop a three-dimensional mesh generator.

## 6 Comparison of the detection algorithms

From the reconstructed datasets we are able to compute the volume fraction of the simulation system that contains defects. This value is plotted in figure 11(a). The shades denote the original data, while the solid and dashed lines are averages over 4000 timesteps. As expected, the volume fraction detected by the mesh generator is larger than the area detected by the pattern recognition algorithm because the mesh generation algorithm's resolution is limited by the size of a unit cell. In addition, the mesh generator detects very small and short-lived variations of the dataset which occur due to small local variations of the gyroid structure resulting in more noisy data for the volume fraction. The results of the pattern recognition algorithm are noisy because the shape of the detected regions is determined by the combination of overlapping squares corresponding to the analysis windows. Small variations of the defect shape can result in differently arranged overlapping windows and thus in varying defect volume fractions. Improvement is possible by using a higher resolution for the pattern recognition analysis, but at greater computational cost. However, both methods show the same general behaviour.

Figure 11(b) shows the averaged volume fraction contained in the large defect in the centre of the system. We compute the total volume of an individual defect by

assuming that all detected areas that overlap belong to the same defect. While for early simulation times, the mesh generator's results fluctuate substantially more than the values obtained from the pattern recognition algorithm, they eventually converge for  $t > 600000$ .

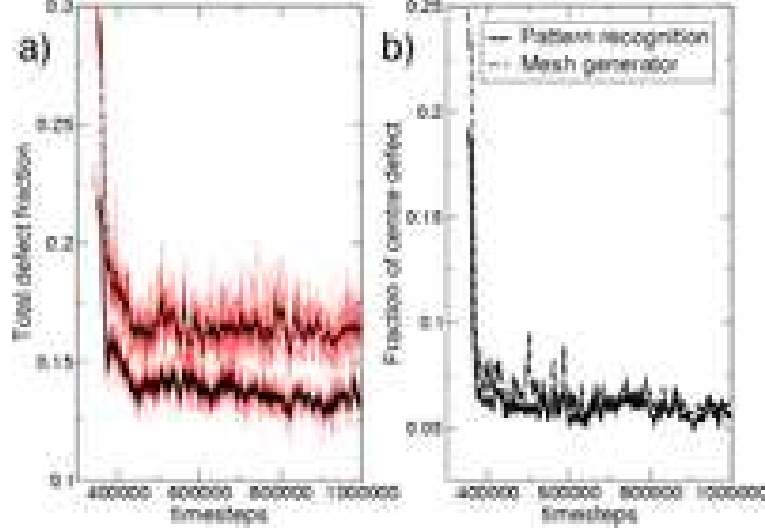


Fig. 11. Fraction of the total simulation volume contained in defects (a) and volume fraction of the large central defect (b) detected by both algorithms. The lighter noisy plots in (a) denote the original data from the pattern recognition algorithm and the mesh generator. The solid and dashed lines have been averaged over 4000 timesteps for better visibility.

An important feature of both algorithms is the possibility they provide to track individual defects in time and so enable us to study their dynamics on the lattice. As an example, we plot the distance of the centre of mass of the large defect in the centre of the system in figure 12. Both methods generate the same general behaviour and differences in these plots are caused by the slightly different volumes detected by both methods. The origin corresponds to the lower front corner in figures 7 and 10.

Finally, we analyse the number of defects detected by both methods for  $t > 34000$ . As shown in table 1, the pattern recognition algorithm has a minimum detection rate of 4 defects which corresponds to a value at an early simulation time ( $t = 346200$ ) and a maximum value of 34 ( $t = 578600$ ). The mean is 20.17 and the standard deviation  $\sigma$  is 3.48. All values are substantially smaller than the results obtained from the mesh generator (see table 1). This is because of the mesh generator's ability to detect very small variations of the gyroid. Furthermore, since the pattern recognition's resolution is limited due to the rectangular shape of the analysis windows, the resulting detection areas are not as flexible in shape as the ones from the mesh generator. Thus, the mesh generator might detect multiple small defects which are very close to each other while the pattern recognition algorithm would detect those as a single defect. We can enhance the comparability of both methods by applying a filter to the mesh generator and only taking defects into account that have a lifetime of at least 1000 timesteps. For our data, the new minimum drops to 7 which is only 3 defects more than obtained using the pattern recognition algorithm. The resulting

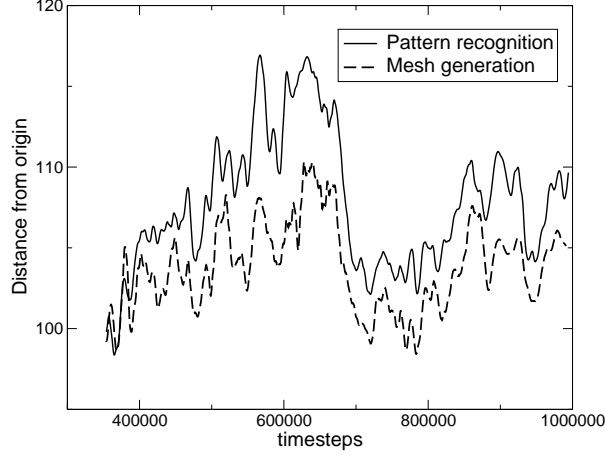


Fig. 12. Distance (in lattice sites) of the centre of the large defect in the centre of the simulated  $128^3$  system from the origin. The data has been obtained using the pattern recognition algorithm (solid line) and the mesh generation algorithm (dashed line). The origin corresponds to the left front corner in figures 7 and 10.

maximum is 36 and the mean becomes 22.76.

Algorithm	Minimum	Maximum	Mean	$\sigma$
Pattern recognition	4	34	20.17	3.48
Mesh generator	28	78	48.70	7.52
Mesh generator (avg)	7	36	22.76	3.80

Table 1

Statistics for the number of defects within the system obtained from the pattern recognition algorithm, the mesh generator and the mesh generator with added time averaging over 4000 timesteps.

In order to make the advantages of the two-dimensional projections apparent, we have extended the pattern recognition algorithm to three dimensions and applied it to the three-dimensional dataset directly. For the case presented here, the computational effort needed to analyse a single dataset is 2.7 times higher than the analysis of all individual projections ( $s=8$ ) in all three directions. Furthermore, the three-dimensional approach does not allow a greater resolution than the size of the analysis window which in our case is  $17 \times 17 \times 17$ . The projection based approach allows us to improve the resolution since the individual two-dimensional windows are mapped to  $17 \times 17 \times 8$  volumes. By taking all three cartesian directions into account, we are able to achieve an effective resolution of  $8 \times 8 \times 8$ . Furthermore, due to the well defined structures produced by the projection algorithm, the detection rate of the pattern recognition algorithm is higher than if one uses it on a non-processed dataset.

## 7 Conclusions

We first briefly described the most spectacular liquid crystalline mesophases which may arise in amphiphilic fluids, and our capability to simulate these. The specific liquid crystalline mesophase of interest has been the cubic gyroid phase. We then described two powerful algorithms based on a pattern recognition algorithm and a mesh generation method to detect and track defects in liquid crystals and applied them to simulation data of a gyroid mesophase obtained during the Ter-aGyroid project [37]. Both algorithms are superior to fully three-dimensional approaches since they exploit basic properties of the system to be analysed. The two-dimensional projection of slabs which have the thickness of a crystal unit cell allows us to reduce the computational analysis effort substantially. Since the pattern recognition algorithm was not developed with gyroid mesophases in mind, it should be applicable to many different regular structures. Additionally, it is more robust in detecting defective areas than the mesh generation algorithm. However, the latter is about ten times faster and thus saves a substantial amount of CPU time if one has to analyse large amounts of simulation data. In addition, we found that time averaging is efficient in filtering out short time fluctuations or artefacts.

The methods described in this paper are most powerful if they are applied in a combined fashion and it would be a natural extension to perform parts of it during an ongoing simulation. For checking if a gyroid phase has formed, observing the variation of the maxima of the projected structure function of the order parameter is most efficient. Efficient parallel FFT implementations are widely available and can be implemented within the simulation code. If the variation of the maxima of the projected structure function drops below a threshold value, one should apply the mesh generation algorithm and track values like the total defect volume or the number of defects. Since our simulation code uses spatial domain decomposition, each CPU can generate the two-dimensional projections of the order parameter individually following which the mesh generation algorithm can be applied locally. The computational effort for this analysis is negligible compared to the actual simulation time, and moreover would allow the scientist to use computational steering techniques [38,46,47] to monitor the state of the simulation while it is running.

The pattern recognition algorithm is less efficient than mesh generation, but is the only choice if one is not limited to simulations of gyroid mesophases. In the gyroid case, it is more efficient to use the results from the mesh generator to select a smaller number of datasets for post-processing using the pattern recognition algorithm since the computational effort involved in the pattern recognition can be substantial. For very large datasets, a promising approach is to determine regions of interest within a single dataset using the mesh generation algorithm and then to analyse subdomains of the system utilizing the pattern recognition approach.

Articles are currently in preparation which make extensive use of the detection

and tracking algorithms described here in order to understand the dynamics and properties of amphiphilic gyroid phases.

## Acknowledgements

We would like to thank Nérido González-Segredo for fruitful discussions and Dmitry Chetverikov for providing the two-dimensional version of the “The IPAN Structural Defect Detector”. We would also like to thank him for his support when we extended it to three dimensions.

We are grateful to the U.K. Engineering and Physical Sciences Research Council (EPSRC) for funding much of this research through RealityGrid grant GR/R67699 and to EPSRC and the National Science Foundation (NSF) for funding the TeraGyroid project.

## References

- [1] J. M. Seddon and R. H. Templer. *Polymorphism of Lipid-Water Systems*, chapter 3, pp 97–160. Elsevier Science B. V., 1995.
- [2] J. M. Seddon and R. H. Templer. Cubic Phases of Self-Assembled Amphiphilic Aggregates. *Phil. Trans.: Phys. Sci. Eng.*, 344(1672):377–401, August 1993.
- [3] C. Czeslik and R. Winter. Structure of water confined in the gyroid cubic phase of the lipid monoelaidin. *J. Mol. Liq.*, 98:283–291, 2002.
- [4] H. Karcher and K. Polthier. Construction of Triply Periodic Minimal Surfaces. *Phil. Trans. R. Soc. Lond. A*, 354(1715):2077–2104, 1996.
- [5] E. A. Lord and A. L. Mackay. Periodic minimal surfaces of cubic symmetry. *Cur. Sci.*, 85(3):346–362, 2003.
- [6] T. A. Shefelbine, M. E. Vigild, M. W. Matsen, D. A. Hajduk, M. A. Hillmyer, E. L. Cussler, and F. S. Bates. Core-Shell Gyroid Morphology in a Poly(isoprene-block-styrene-block-dimethylsiloxane) Triblock Copolymer. *J. Am. Chem. Soc.*, 121(37):8457–8465, 1999.
- [7] T. Landh. From entangled membranes to eclectic morphologies: cubic membranes as subcellular space organizers. *FEBS Lett.*, 369(1):13–17, 1995.
- [8] A. Schoen. Infinite Periodic Minimal Surfaces Without Self-Intersections. *NASA Tech. Note*, D-5541, Washington, DC, 1970.
- [9] K. Große-Brauckmann. Gyroids of Constant Mean Curvature. *Exp. Math.*, 6(1):33–50, 1997.

- [10] P. J. F. Gandy and J. Klinowski. Exact computation of the triply periodic G ('Gyroid') minimal surface. *Chem. Phys. Lett.*, 321(5):363–371, 2000.
- [11] A. Fogden and S. T. Hyde. Continuous transformations of cubic minimal surfaces. *Eur. Phys. J. B*, 7(1):91–104, 1999.
- [12] P. G. de Gennes and J. Prost. *Physics of Liquid Crystals*. Oxford University Press, second edition, 1995.
- [13] D. Frenkel and R. Eppenga. Monte Carlo Study of the Isotropic-Nematic Transition in a Fluid of Thin Hard Disks. *Phys. Rev. Lett.*, 79(15):1089–1092, 1982.
- [14] M. P. Allen. Molecular simulation and theory of liquid crystal surface anchoring. *Mol. Phys.*, 96(9):1391–1397, 1999.
- [15] M. P. Allen and M. A. Warren. Molecular-dynamics simulation of the smectic-A\* twist grain-boundary phase. *Phys. Rev. E*, 57(5):5585–5596, 1998.
- [16] G. Gompper and M. Schick. Self-assembling amphiphilic systems. In C. Domb and J. Lebowitz, editors, *Phase Transitions and Critical Phenomena*, volume 16, pp 1–176. Academic Press, 1994.
- [17] A. Ciach and R. Holyst. Periodic surfaces and cubic phases in mixtures of oil, water, and surfactant. *J. Comp. Phys.*, 110(6):3207–3214, 1999.
- [18] R. Holyst and P. Oswald. Confined complex liquids: Passages, droplets, permanent deformations, and order-disorder transitions. *J. Comp. Phys.*, 109(24):11051–11060, 1998.
- [19] U. S. Schwartz and G. Gompper. Stability of Inverse Bicontinuous Cubic Phases in Lipid-Water Mixtures. *Phys. Rev. Lett.*, 85(7):1472–1475, 2000.
- [20] S. Succi. *The Lattice Boltzmann Equation for Fluid Dynamics and Beyond*. Oxford University Press, 2001.
- [21] Y. H. Qian, D. d'Humières, and P. Lallemand. Lattice BGK Models for Navier-Stokes Equation. *Europhys. Lett.*, 17(6):479–484, 1992.
- [22] P. J. Love, M. Nekovee, P. V. Coveney, J. Chin, N. González-Segredo, and J. M. R. Martin. Simulations of amphiphilic fluids using mesoscale lattice-Boltzmann and lattice-gas methods. *Comp. Phys. Comm.*, 153:340–358, 2003.
- [23] C. M. Care, I. Halliday, and K. Good. Lattice Boltzmann nemato-dynamics. *J. Phys. Condens. Matter*, 12(43):L665–L671, 2000.
- [24] M. R. Swift, E. Orlandini, W. R. Osborn, and J. M. Yeomans. Lattice-Boltzmann simulations of liquid-gas and binary fluid mixtures. *Phys. Rev. E*, 54(5):5041–5052, 1996.
- [25] E. Orlandini, M. R. Swift, and J. M. Yeomans. A Lattice Boltzmann Model of Binary-Fluid Mixtures. *Europhys. Lett.*, 32(6):463–468, 1995.
- [26] M. R. Swift, W. R. Osborn, and J. M. Yeomans. Lattice Boltzmann Simulation of Nonideal Fluids. *Phys. Rev. E*, 75(5):830–833, 1995.

- [27] C. Denniston, D. Marenduzzo, E. Orlandini, and J. M. Yeomans. Lattice Boltzmann Algorithm for three-dimensional liquid crystal hydrodynamics. *Phil. Trans. R. Soc. Lond. A*, 362(1821):1745–1754, 2004.
- [28] C. Denniston, E. Orlandini, and J. M. Yeomans. Simulations of Liquid Crystal hydrodynamics. *Europhys. Lett.*, 52(4):481–487, 2000.
- [29] C. Denniston, E. Orlandini, and J. M. Yeomans. Lattice Boltzmann simulations of liquid crystal hydrodynamics. *Phys. Rev. E*, 63(056702), 2001.
- [30] O. Theissen, G. Gompper, and D. M. Kroll. Lattice-Boltzmann Model of Amphiphilic Systems. *Europhys. Lett.*, 42:419–414, 1998.
- [31] A. Lamura, G. Gonnella, and J. M. Yeomans. A Lattice-Boltzmann Model of Ternary Fluid Mixtures. *Europhys. Lett.*, 45(3):314–320, 1999.
- [32] X. Shan and H. Chen. Lattice Boltzmann model for simulating flows with multiple phases and components. *Phys. Rev. E*, 47(3):1815–1819, 1993.
- [33] N. S. Martys and J. F. Douglas. Critical properties and phase separation in lattice Boltzmann fluid mixtures. *Phys. Rev. E*, 63:031205, 2001.
- [34] H. Chen, B. M. Boghosian, P. V. Coveney, and M. Nekovee. A Ternary Lattice Boltzmann Model for Amphiphilic Fluids. *Proc. R. Soc. Lond. A*, 456:2043–2047, 2000.
- [35] N. González-Segredo and P. V. Coveney. Self-assembly of the gyroid cubic mesophase: lattice-Boltzmann simulations. *Europhys. Lett.*, 65(6):795–801, 2004.
- [36] N. González-Segredo and P. V. Coveney. Coarsening dynamics of ternary amphiphilic fluids and the self-assembly of the gyroid and sponge mesophases: lattice-Boltzmann simulations. *Phys. Rev. E*, 69:061501, 2004.
- [37] S. M. Pickles, R. J. Blake, B. M. Boghosian, J. M. Brooke, J. Chin, P. E. L. Clarke, P. V. Coveney, R. Haines, J. Harting, M. Harvey, N. González-Segredo, M. A. S. Jones, M. McKeown, R. K. Pinning, A. R. Porter, K. Roy, and M. Riding. The TeraGyroid Experiment. *Proceedings of the Workshop on Case Studies on Grid Applications at GGF 10*, 2004. Available online: <http://www.zib.de/ggf/apps/meetings/ggf10.html>.
- [38] J. Chin, J. Harting, S. Jha, P. V. Coveney, A. R. Porter, and S. M. Pickles. Steering in computational science: mesoscale modelling and simulation. *Contemporary Physics*, 44(5):417–434, 2003.
- [39] The RealityGrid project: <http://www.RealityGrid.org>.
- [40] The TeraGyroid project: <http://www.RealityGrid.org/TeraGyroid.html>.
- [41] N. González-Segredo, M. Nekovee, and P. V. Coveney. Three-dimensional lattice-Boltzmann simulations of critical spinodal decomposition in binary immiscible fluids. *Phys. Rev. E*, 67(046304), 2003.
- [42] D. A. Hajduk, P. E. Harper, S. M. Gruner, C. C. Honeker, G. Kim, and E. L. Thomas. The Gyroid: A New Equilibrium Morphology in Weakly Segregated Diblock Copolymers. *Macromolecules*, 27:4063, 1994.

- [43] J. H. Laurer, D. A. Hajduk, J. C. Fung, J. W. Sedat, S. F. Smith, S. M. Gruner, D. A. Agard, and R. J. Spontak. Microstructural Analysis of a Cubic Bicontinuous Morphology in a Neat SIS Triblock Copolymer. *Macromolecules*, 30:3938, 1997.
- [44] D. Chetverikov and A. Hanbury. Finding defects in texture using regularity and local orientation. *Pattern Recognition*, 35:203–218, 2002. An online demo of the algorithm is available at <http://aramis.ipan.sztaki.hu/strucdef/strucdef.html>.
- [45] D. Chetverikov. Pattern regularity as a visual key. *Image and Vision Computing*, 18:975–985, 2000.
- [46] J. M. Brooke, P. V. Coveney, J. Harting, S. Jha, S. M. Pickles, R. L. Pinning, and A. R. Porter. Computational Steering in RealityGrid. In *Proceedings of the UK e-Science All Hands Meeting, September 2-4, 2003*. (<http://www.nesc.ac.uk/events/ahm2003/AHMCD/pdf/179.pdf>).
- [47] J. Harting, M. Venturoli, and P. V. Coveney. Large-scale grid-enabled lattice-Boltzmann simulations of complex fluid flow in porous media and under shear. *Phil. Trans. R. Soc. Lond. A*, 362:1703–1722, 2004.